A thermal pressurization model for the spontaneous dynamic rupture propagation on a three-dimensional fault: 2. Traction evolution and dynamic parameters

A. Bizzarri[1,2] and M. Cocco[1]

[1]   We investigate the dynamic traction evolution during the spontaneous propagation of a 3-D earthquake rupture governed by slip-weakening or rate- and state-dependent constitutive laws and accounting for thermal pressurization effects. The analytical solutions as well as temperature and pore pressure evolutions are discussed in the companion paper by Bizzarri and Cocco. Our numerical experiments reveal that frictional heating and thermal pressurization modify traction evolution. The breakdown stress drop, the characteristic slip-weakening distance, and the fracture energy depend on the slipping zone thickness ($2w$) and hydraulic diffusivity (ω). Thermally activated pore pressure changes caused by frictional heating yield temporal variations of the effective normal stress acting on the fault plane. In the framework of rate- and state-dependent friction, these thermal perturbations modify both the effective normal stress and the friction coefficient. Breakdown stress drop, slip-weakening distance, and specific fracture energy (J/m^2) increase for decreasing values of hydraulic diffusivity and slipping zone thickness. We propose scaling relations to evaluate the effect of w and ω on these physical parameters. We have also investigated the effects of choosing different evolution laws for the state variable. We have performed simulations accounting for the porosity evolution during the breakdown time. Our results point out that thermal pressurization modifies the shape of the slip-weakening curves. For particular configurations, the traction versus slip curves display a gradual and continuous weakening for increasing slip: in these cases, the definitions of a minimum residual stress and the slip-weakening distance become meaningless.

1.   Introduction

[2]   The dynamic fault weakening during the propagation of an earthquake rupture is represented by the traction evolution within the cohesive zone: after an initial increase caused by the dynamic load, total traction drops from the upper yield stress (τ_u) to the kinetic or residual stress level (τ_f) during a time interval defining the breakdown time in which slip reaches the characteristic slip-weakening distance (d_0) (see Figure 1). In this study we refer to the cohesive or breakdown zone as the zone of shear stress degradation near the tip of a propagating rupture. It is important to emphasize that the existence of the breakdown zone and the evaluation of its dimension rely on the identification of the residual kinetic stress and the characteristic slip-weakening distance. Many

investigators have pointed out that the shape of the slip-weakening curve (SW; i.e., total dynamic traction versus cumulative slip) as well as the temporal evolution of dynamic traction can be complex and nonlinear [*Campillo and Ionescu*, 1997; *Mair and Marone*, 1999; *Abercrombie and Rice*, 2005]. Many different physical processes can yield this traction evolution, as revealed by laboratory [*Okubo and Dieterich*, 1984; *Ohnaka et al.*, 1987; *Mair and Marone*, 1999] and numerical experiments [*Cocco and Bizzarri*, 2002; *Andrews*, 2002]. *Bizzarri and Cocco* [2003] have shown that rate- and state-dependent (RS in the following) friction laws yield a traction evolution consistent with the SW behavior and have proposed scaling relations to associate the constitutive and stress parameters. *Ohnaka* [2003] points out that because of the complexities of the slipping zones and the roughness of the sliding surfaces, shear traction and cumulative slip should be considered as macroscopic averages of more complex and highly localized processes affecting fault friction and fracture.

[3]   The main physical parameters characterizing the traction evolution within the cohesive zone (see Figure 1) are the breakdown stress drop $\Delta\tau_b$ (defined as ($\tau_u - \tau_f$)), the

---

[1]Istituto Nazionale di Geofisica e Vulcanologia, Sezione di Sismologia e Tettonofisica, Rome, Italy.
[2]Now at the Istituto Nazionale di Geofisica e Vulcanologia, Sezione di Bologna, Bologna, Italy.
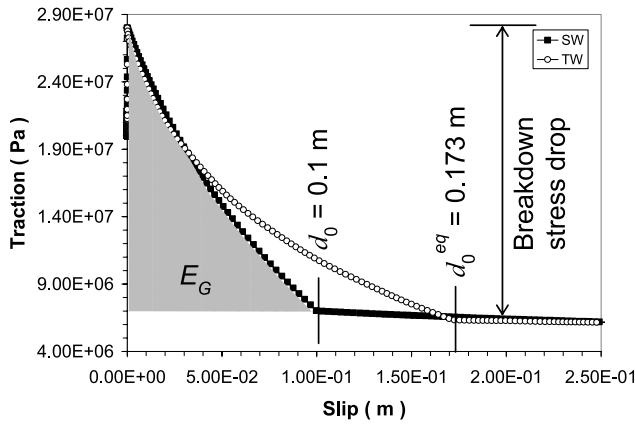
Figure 1. Slip-weakening curves for two different wet configuration. Solid symbols refer to the reference configuration with a SW law; open symbols refer to a TW friction law, in which the fault friction decreases linearly with increasing time. Solutions are plotted in a fault point at a distance of 900 m from the hypocenter, at the depth of the hypocenter; this point is far enough from the nucleation patch to be unaffected by the imposed nucleation. Medium and constitutive parameters are listed in Table 1 of BC06.

characteristic SW distance and the specific (i.e., per unit area) energy (E_G), which is

$$E_G \underset{\mathrm{df}}{=} \int_0^{d_0} \left(\tau(u) - \tau_f \right) du \qquad (1)$$

where u is the fault slip. In the case of RS governing law d_0 and τ_f have to be regarded as "equivalent" quantities, following *Bizzarri and Cocco* [2003]. *Palmer and Rice* [1973], and subsequently many others, have called this quantity fracture energy (G; more properly fracture energy density). More recently, *Tinti et al.* [2005] have proposed to call the same quantity breakdown work (formally a work density), because this is a more general term which accounts for the unknown combination of surface energy and heat. Recent investigations suggest that both the SW distance and fracture energy are scale-dependent quantities [see *Ohnaka*, 2003]; in this case, they should not be considered as constitutive parameters dependent on material properties.

[4] In this study we aim to interpret the traction evolution inferred by modeling the dynamic propagation of an earthquake rupture on a fault governed by thermal pressurization and to discuss how frictional heating and fluid flow can affect the estimates of the main physical parameters. In the companion paper [*Bizzarri and Cocco*, 2006] (hereinafter referred to as BC06) we have analytically solved the 1-D thermal pressurization problem taking into account different constitutive relations representing fault friction and including the temporal evolution of the effective normal stress. We have calculated the temperature and the pore pressure changes on the fault plane caused by the spontaneous propagation of a 3-D fully dynamic, truly 3-D rupture using different values of the slipping zone thickness and hydraulic diffusivity. The simulations presented and discussed in

BC06 show that thermal pressurization with constant porosity is able to modify the dynamic rupture propagation (i.e., the rupture velocity and the shape of the rupture front) as well as the temporal evolution of the friction coefficient. The aim of the present paper is to explore and discuss in detail how thermal pressurization modifies the main physical parameters characterizing the traction evolution: the breakdown stress drop, the characteristic SW distance and the fracture energy. We also discuss the effects of time-dependent porosity, although a complete discussion of porosity evolution is beyond the goals of the present study. Moreover, we emphasize that the proper way to represent analytically the evolution of porosity due to the dynamic rupture is the largest unknown in all theoretical models of thermal pressurization.

[5] *Fialko* [2004] has presented an interesting discussion on the thermal perturbation caused by coseismic slip during the dynamic propagation of a 2-D crack having a prescribed constant yield stress level within the cohesive zone [see *Fialko*, 2004, Figure 4]. Although using a nonspontaneous 2-D model and a simplified traction evolution within the cohesive zone, this author also discusses the coseismic temperature increase generated by a self-healing pulse of slip velocity. *Andrews* [2002] solved a 3-D problem using an analytical relation for the heat source (in other words, he did not solve the 1-D heat conduction equation as *Fialko* [2004] and BC06) and a time-weakening friction evolution within the cohesive zone; in his calculations friction does not drop abruptly to the kinetic stress level, but the transition from static to kinetic friction occurs in a specified (and short) time interval (see Figure 1). The goal of our study is to model and discuss the spontaneous traction evolution in a 3-D dynamic model governed either by SW or RS friction laws and including thermal pressurization effects. Thus we extend the analysis of *Andrews* [2002] by considering different constitutive laws which allows us to discuss more in detail the traction evolution.

[6] Figure 1 shows an example of total dynamic traction evolution as a function of slip obtained by using a slip- and a time-weakening (TW) constitutive relations and including thermal pressurization with constant porosity. These solutions have been obtained by assuming a half thickness of the slipping zone of 35 mm and a hydraulic diffusivity value of 0.02 m²/s. In these simulations the characteristic time for shear stress degradation in the time-weakening model (t_0; the time required to drop shear traction from its maximum value to the residual level) is 0.07 s, while the characteristic distance for a SW model is 0.1 m (all the other constitutive and model parameters are the same, see Table 1 of BC06). Our calculations performed with the TW model agree with those presented by *Andrews* [2002, Figure 4], corroborating our numerical results. Figure 1 points out that because the residual stress level is imposed a priori (also the characteristic slip-weakening distance in a SW simulation), thermal pressurization with constant porosity causes a nonlinear traction decay for slip amplitudes ranging between 0 and d_0. The main difference using a SW friction law from RS is that in the former case the traction is prescribed a priori, while in the latter total dynamic traction spontaneously evolves during sliding. In the following, we compare RS and SW constitutive laws in order to discuss the effects of
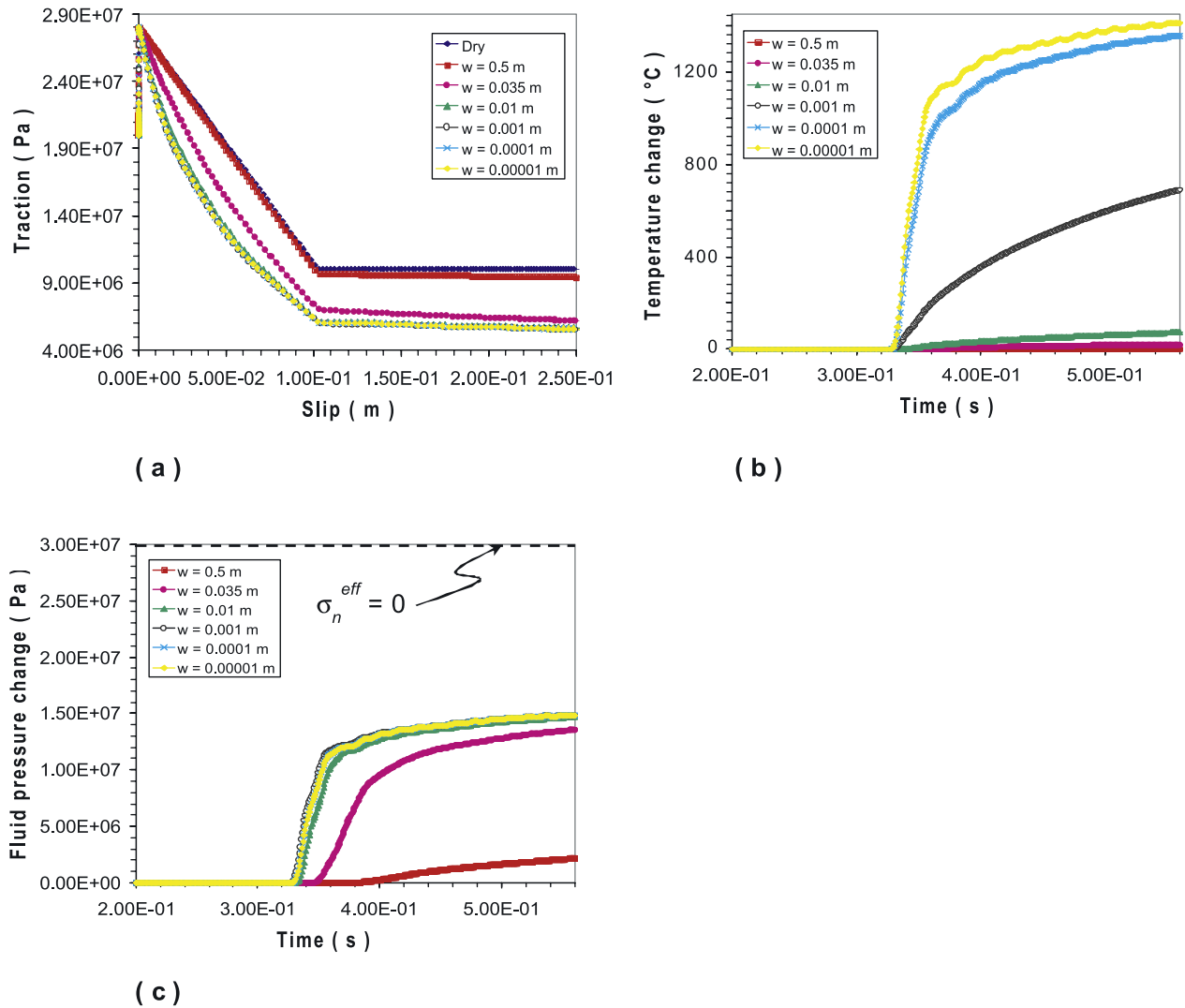
Figure 2. Solutions for various wet faults obeying to a linear SW friction law and having different slipping zone half thickness w. Results for the reference dry case is plotted for comparison. (a) Slip-weakening curve. (b) Temperature change (with respect to its initial value T_0^f) as a function of time. (c) Fluid pressure change (with respect to its initial value $p_{fluid_0}^f$) as a function of time. Solutions are plotted in the same fault point selected in Figure 1.

temperature and pore pressure changes on the dynamic traction evolution.

2. Simulations With a Slip-Weakening Law

[7]   We first discuss the dynamic traction evolution for a fault obeying a SW law. We define "dry" the fault for which there is no thermal pressurization and we consider this as our reference configuration. We refer to "wet" faults for all the other configurations in which thermal pressurization is taken into account. All the parameters adopted in this paper are the same (unless otherwise specified) and are listed in Table 1 of BC06, where we have also described the model parameterization; the numerical approach is the Finite Difference code used in BC06 and described in detail by *Bizzarri and Cocco* [2005, and references therein].

[8]   Figures 2 and 3 show the slip-weakening curves, the temperature and pore pressure changes for several simula-tions performed using different values of the slipping zone half thickness (w) and the hydraulic diffusivity (ω). All the other parameters are fixed in these numerical experiments and these simulations have been performed assuming a constant porosity. In section 7 we discuss the effects of dynamic porosity evolution. The hydraulic diffusivity val-ues used in our simulations are in agreement with those adopted by *Miller* [2002] and with the values inferred for tectonic environments [*Manning and Ingebritsen*, 1999]. The temperature and pore pressure changes are discussed in detail by *Bizzarri and Cocco* [2006]. We remark here that fluid pressure decreases for increasing the thickness of the slipping zone; for thin slipping zones ($w \leq 1$ mm, for the model parameters used in this study) the effective normal stress (σ_n^{eff}) is reduced by nearly 50%. The temperature increase and the effective normal stress reduction are even larger for small values of the hydraulic diffusivity ($\omega \leq 0.01$ m^2/s). This means that for large slip zone thickness the

(a)

(b)

(c)
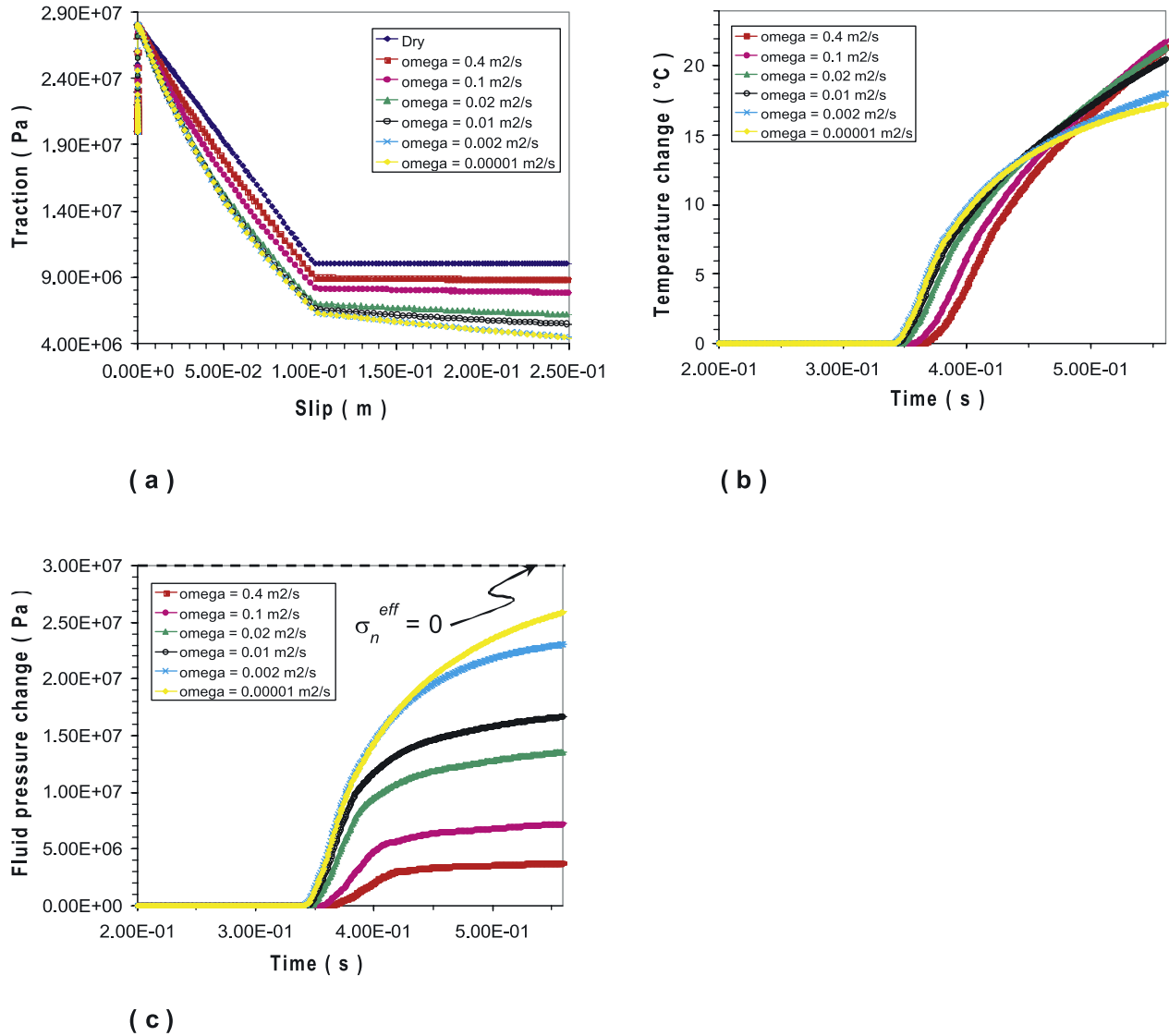
Figure 3. Same as Figure 2, but changing the hydraulic diffusivity and keeping fixed the slipping zone thickness equal to the reference value (see Table 1 of BC06). We change ω by varying the permeability k. Solutions are plotted in the same fault point of Figure 2.

thermal pressurization effects are less important, in agreement with the results of *Noda and Shimamoto* [2005], who used a nonspontaneous fault model with constant friction coefficient, following *Lachenbruch* [1980]. The decrease in effective normal stress determines a decrease in the residual stress level and, consequently, a reduction of the effective strength parameter S [*Das and Aki*, 1977a, 1977b]. A decrease in the S parameter causes larger peaks of slip velocity. This also implies larger breakdown stress drop values $(\tau_u - \tau_f)$ for a thin fault and for small values of hydraulic diffusivity. All these effects are relevant to the dynamic traction evolution (see Figures 2a and 3a); the simulations performed by assuming a SW law have a fixed characteristic slip-weakening distance (indeed d_0 is assumed a priori) and a constant (unaffected) yield stress value (τ_u), because at the time in which dynamic traction reaches its peak value frictional heating and thermal pressurization do not have an effect on traction evolution, as expected from equation (9) of BC06. Figures 2 and 3 have been computed

for a determined drop of friction coefficient during dynamic fault weakening in dry conditions ($\mu_u = 0.93333$ and $\mu_f = 0.33333$, corresponding to a strength parameter value S equal to 0.8). In the following, we compare these results with other calculations performed with different values of the strength parameter.

[9] These simulations reveal that thermal pressurization with a constant porosity slightly change the weakening rate with cumulative fault slip $(\partial\tau/\partial u)$ when a SW law is adopted; it becomes nonlinear and convex for small slipping zone thickness ($w \leq 1$ mm, for the parameter set used in this study). These changes slightly modify the fracture energy (equation (1)) estimates yielding a crack tip bifurcation and acceleration to supershear rupture velocities [see *Bizzarri and Cocco*, 2005; BC06]. It is important to emphasize that in the case of a SW law, thermal pressurization affects the dynamic traction evolution only through changes in the effective normal stress, since the friction coefficient does not vary with time in this constitutive formulation. This is a

relevant difference with the simulations performed with RS, where we expect to obtain larger modifications of the dynamic traction evolution caused by thermal pressurization. We discuss this in section 3.

3. Simulations With Rate- and State-Dependent Friction Laws

[10] In this section we discuss the results of several numerical experiments performed by adopting the RS constitutive laws presented in BC06. For completeness we write again here the constitutive equations. We use two different friction laws; the first one is the ageing law proposed by *Linker and Dieterich* [1992] and named DR in BC06 and hereinafter

$$
\begin{aligned}
\tau &= \left[\mu_* + a \ln\left(\frac{v}{v_*}\right) + b \ln\left(\frac{\Psi v_*}{L}\right) \right] \sigma_n^{\mathrm{eff}} \\
\frac{\mathrm{d}}{\mathrm{d}t}\Psi &= 1 - \frac{\Psi v}{L} - \left(\frac{\alpha_{\mathrm{LD}}\Psi}{b\sigma_n^{\mathrm{eff}}}\right)\frac{\mathrm{d}}{\mathrm{d}t}\sigma_n^{\mathrm{eff}}
\end{aligned}
\tag{2}
$$

where a and b and L are the constitutive parameters; μ_* and v_* are reference values for the friction coefficient and for the macroscopic fault slip velocity v, respectively. Ψ is the state variable and α_{LD} is a dimensionless coupling parameter [*Linker and Dieterich*, 1992]. The second constitutive law is the modified slip law [see *Beeler et al.*, 1994], which differs from (2) only for the state variable evolution law and it is named RD in this study:

$$
\begin{aligned}
\tau &= \left[\mu_* + a \ln\left(\frac{v}{v_*}\right) + b \ln\left(\frac{\Psi v_*}{L}\right) \right] \sigma_n^{\mathrm{eff}} \\
\frac{\mathrm{d}}{\mathrm{d}t} &= -\frac{\Psi v}{L} \ln\left(\frac{\Psi v}{L}\right) - \left(\frac{\alpha_{\mathrm{LD}}\Psi}{b\sigma_n^{\mathrm{eff}}}\right)\frac{\mathrm{d}}{\mathrm{d}t}\sigma_n^{\mathrm{eff}}
\end{aligned}
\tag{3}
$$

As in the simulations presented and discussed in section 2, we have performed many numerical experiments using the ageing law defined in (2) (i.e., the Dieterich-Ruina, DR, model) in order to check the influence of the slipping zone thickness $2w$ (Figure 4), of the hydraulic diffusivity ω (Figure 5) and of the dimensionless parameter α_{LD} (Figure 6). We remind here that because the shear traction, the slip and slip velocity are considered as macroscopic quantities, the state variable appearing in relations (2) and (3) should be also considered as a macroscopic average representing complex processes in the slipping zone. We discuss in section 6 the simulations performed using the RD constitutive law defined in (3). The simulations presented in Figures 4, 5, and 6 have been calculated for a constant porosity model.

3.1. Evolution of the State Variable

[11] We have briefly discussed the effects of thermal pressurization on the state variable evolution in BC06 (see

Figure 10 of BC06). In particular, we have shown that the state variable evolution for wet faults is substantially different than that for a dry fault. We discuss here the effect of different slipping zone thickness, hydraulic diffusivity and the dimensionless parameter α_{LD} and we show the results in Figures 4b, 5b, and 6b. These simulations clearly point out that decreasing the slipping zone thickness and the hydraulic diffusivity values produces a sharp increase in the state variable followed by a sudden drop to the new steady state value. The time interval in which the state variable evolves coincides with the breakdown time (i.e., the duration of the dynamic weakening phase); the smaller the values of slipping zone thickness and hydraulic diffusivity the shorter the breakdown time (see Figures 4a, 4b, 5a and 5b). The state variable evolution is smoother for thick slipping zone ($w \geq 0.1$ m) and for large hydraulic diffusivity values ($\omega \geq 0.1$ m^2/s); in these simulations, the state variable gradually decreases from the initial to the final steady state.

[12] As stated in equations (2) and (3), the parameter α_{LD} controls the coupling between the effective normal stress and the state variable evolution. We show in Figure 6 simulation results obtained by using different α_{LD} and adopting values comprised within the range of those experimentally determined by *Linker and Dieterich* [1992]. Figure 6b shows that as α_{LD} increases, the state variable is more sensitive to the variation of σ_n^{eff}; the larger α_{LD} the longer the breakdown time. It is important to point out that the simulation with $\alpha_{\mathrm{LD}} = 0$ (eliminating the effects of σ_n^{eff} on the state variable) is different from the dry configuration and yields the shortest state variable evolution among those illustrated in Figure 6. This is because thermal pressurization with constant porosity affects the total dynamic traction through the temporal changes of effective normal stress (which are absent in a dry configuration). It is likely that different state variable evolution laws will affect the temporal evolution of total dynamic traction as well as the slip-weakening curves, as we discuss in the following.

3.2. Temporal Evolution of Dynamic Traction

[13] Figures 4c, 4d, 5c, 5d, 6c, and 6d depict the temperature and pore pressure changes (with respect the their initial values, T_0^f and $p_{\mathrm{fluid}_0}^f$, respectively) for different slipping zone thickness, hydraulic diffusivity and the dimensionless parameter α_{LD}, while Figures 4a, 5a, and 6a display the temporal evolution of dynamic traction. The thermal perturbations and the fluid pressure changes have been discussed in detail in BC06. We remind here that for the set of parameters used in this study and for a constant porosity, increasing the slip zone thickness, as well as the hydraulic diffusivity, the temperature and the pore pressure changes on the fault are reduced. Figure 6 shows that changing the parameter α_{LD} has a negligible effect on the pore pressure changes and a modest impact on the temperature evolution.

Figure 4. Solutions for different wet faults (we change the slip zone thickness) governed by a Dieterich-Ruina constitutive law; in all plots we have plotted the dry case, for comparison. (a), (b), (c) and (d) Time evolution of traction, state variable, temperature, and fluid pressure, respectively. (e) Slip-weakening curve and (f) phase portrait (i.e., total dynamic traction versus fault slip velocity). In Figure 4e we have reported a zoom of the slip-hardening stage (i.e., increase traction with increasing slip). Solutions are plotted in a fault point located at a distance of 1300 m from the hypocenter.
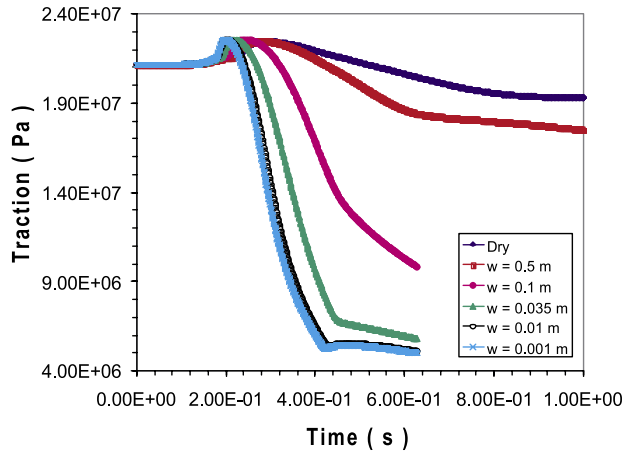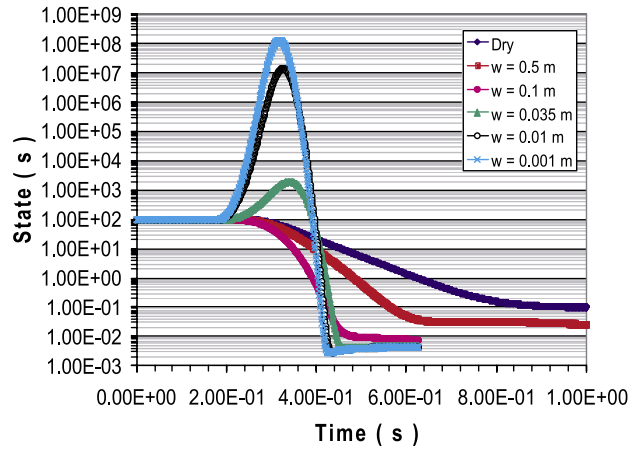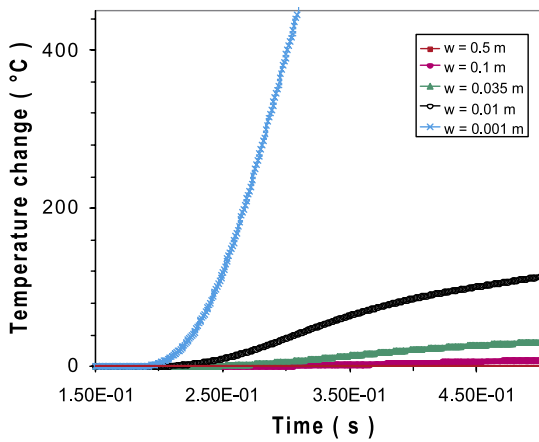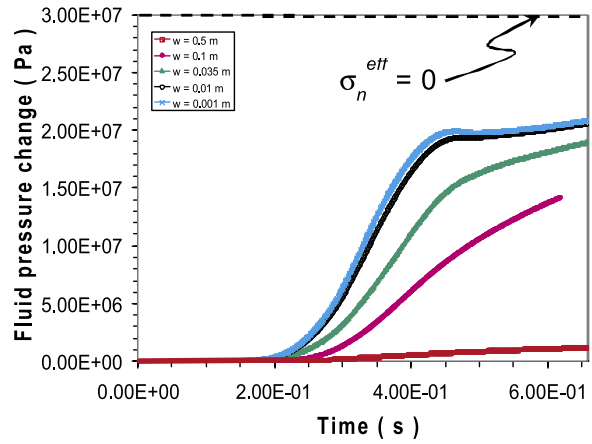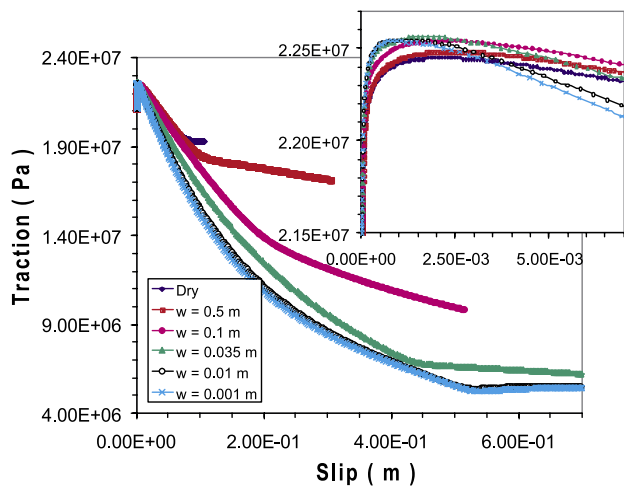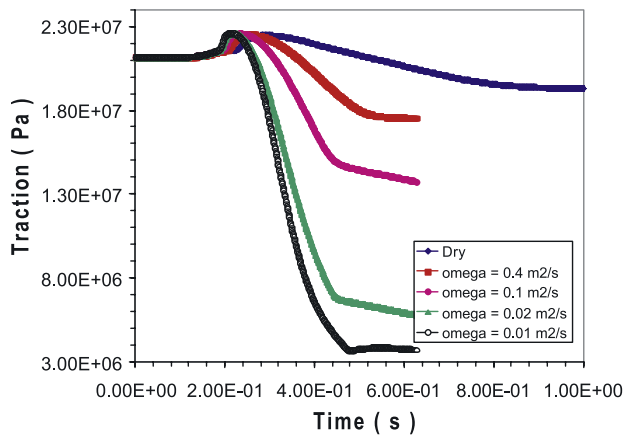
Figure 4
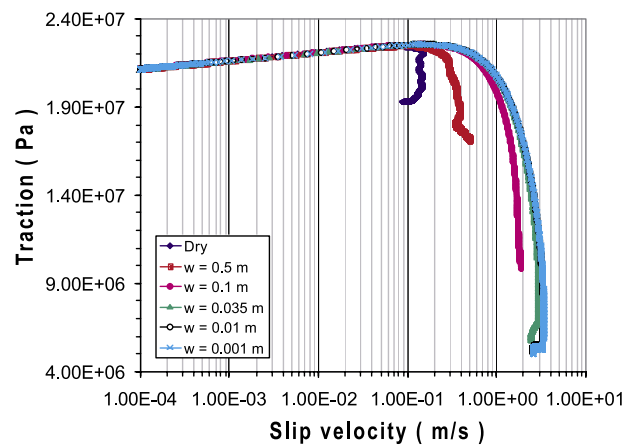
(a)
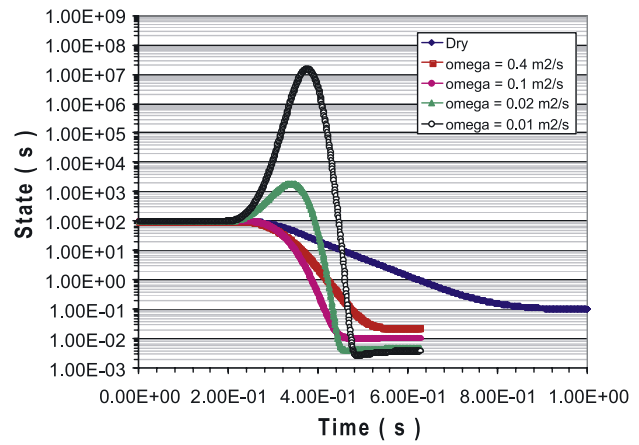
(b)
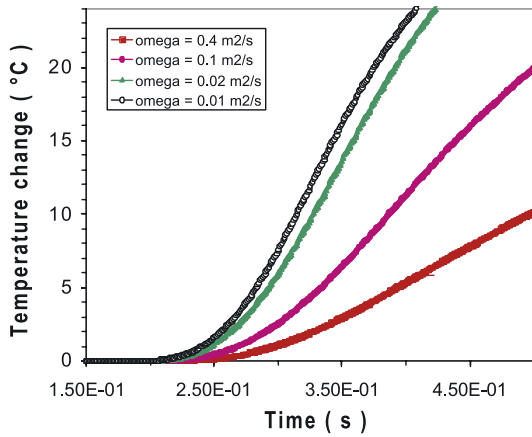
(c)
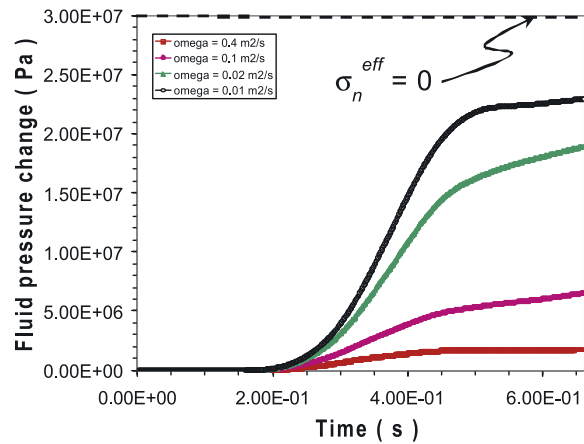
(d)
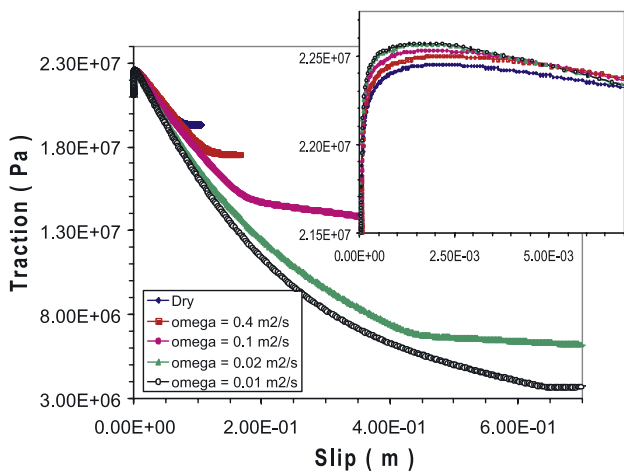
(e)
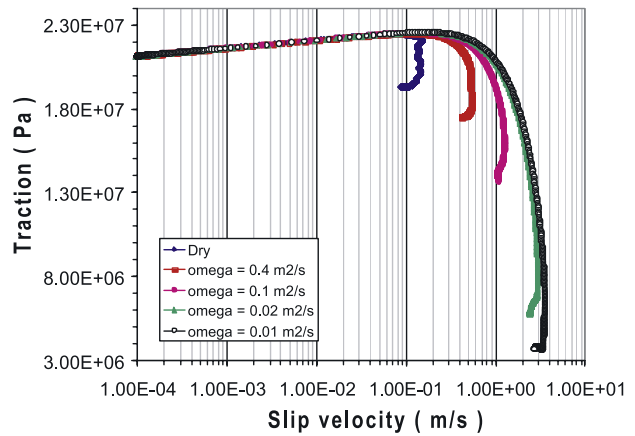
(f)

Figure 5. Same as Figure 4, but changing the hydraulic diffusivity and keeping fixed the slipping zone thickness as the reference value. As in the SW numerical experiments (see Figure 3), we change ω by varying k.
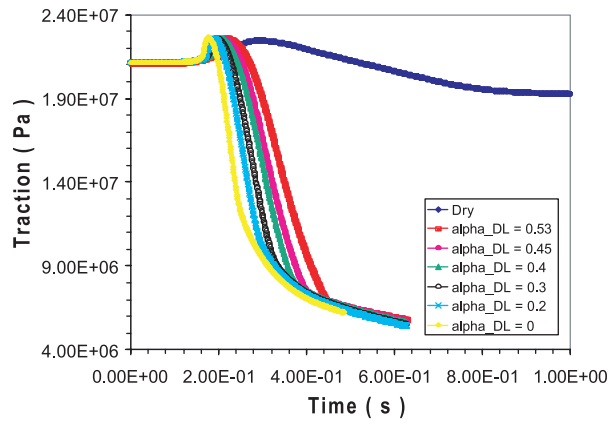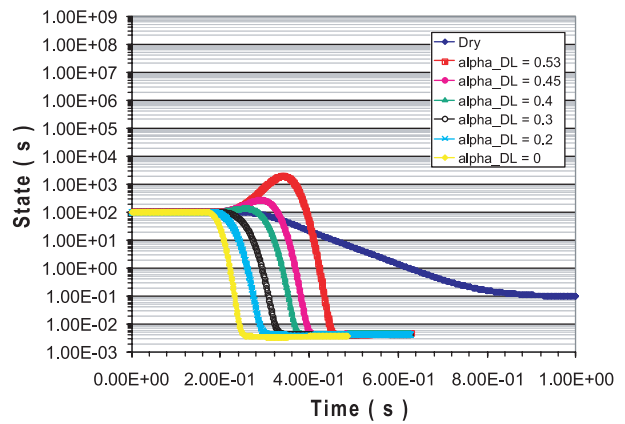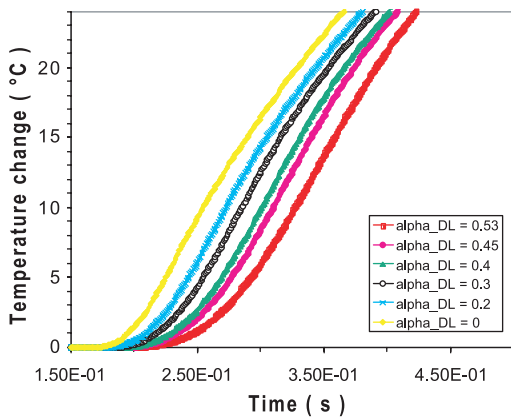
(a)

(b)

(c)
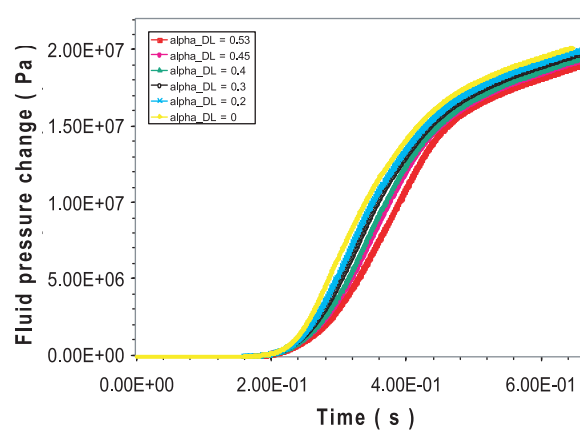
(d)
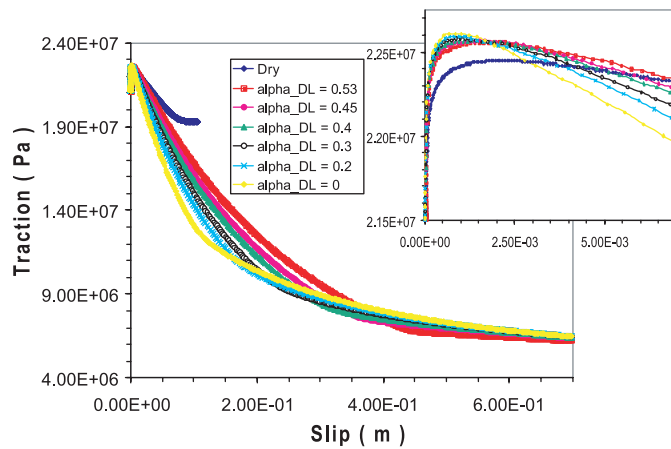
(e)
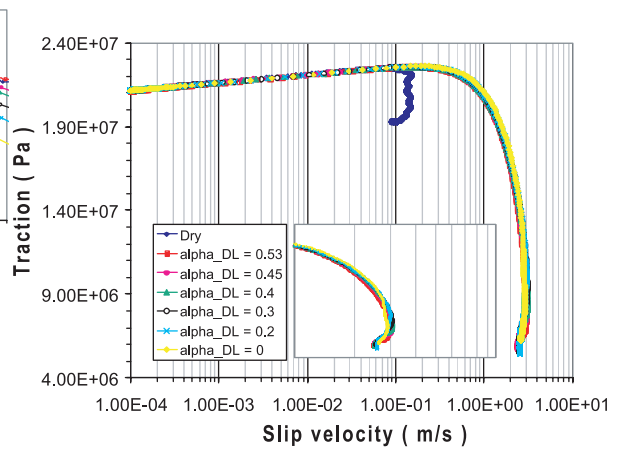
(f)

Figure 6. Same as Figure 5, but for different values of the dimensionless parameter α_{LD} that represent the coupling between effective normal stress changes and state variable temporal evolution. For $\alpha_{LD} = 0$ the evolution equation is identical to that of the dry fault and the effective normal stress variations affect only the value of total dynamic traction through the Terzaghi effective stress laws but not through the state variable evolution. All the other parameters are those listed in Table 1 of BC06. (f) Zoom of the phase diagram to emphasize the behavior at high fault slip velocities.
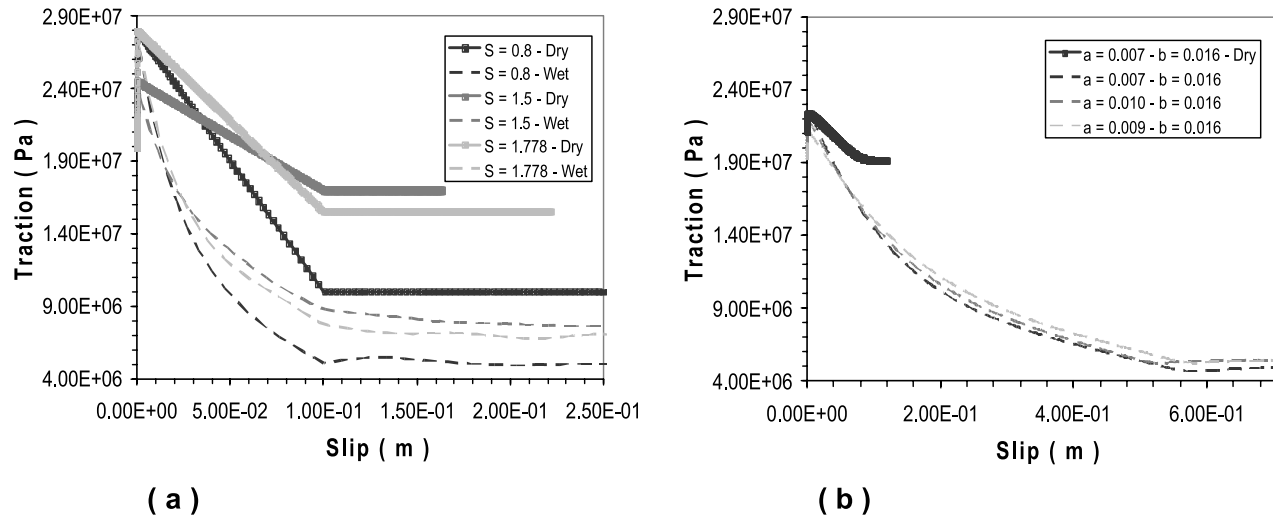
Figure 7. Slip-weakening curves computed adopting (a) a linear SW law and (b) the DR law for different constitutive configurations. For each configuration, solid lines identify simulations performed for dry faults (i.e., no thermal pressurization), and dashed lines identify those for wet faults (with thermal pressurization and constant porosity). These solutions are calculated in a fault point located at a distance of 1875 m from the hypocenter and for a slipping zone half thickness $w = 0.001$ m. The SW simulations have been performed for three values of the strength parameter S: those with $S = 0.8$ represent the reference case, whose constitutive parameters are listed in Table 1. The other two constitutive configurations have $S = 1.5$, corresponding to $\mu_u = 0.81667$ and $\mu_f = 0.56667$, and $S = 1.778$, corresponding to $\mu_u = 0.93333$ and $\mu_f = 0.51667$. The values of a and b parameters used in the simulations with the DR law are indicated in the legend of each panel. All the other parameters are those listed in Table 1 of BC06.

[14] The most interesting result emerging from these simulations concerns the temporal evolutions of total dynamic traction (Figures 4a, 5a, and 6a); thermal pressurization modifies the dynamic fault weakening. Large values of the slipping zone thickness ($\sim$0.5 m) and of the hydraulic diffusivity ($\sim$0.4 m^2/s) yield dynamic traction evolutions quite different from those inferred for a dry fault. This difference is even more evident for the variation of the parameter α_{LD}. Thus we conclude that thermal pressurization with constant porosity modifies: (1) the duration of the dynamic weakening phase, (2) the residual stress level (τ_f^{eq}), (3) the breakdown and the dynamic stress drop ($\tau_0 - \tau_f$, where τ_0 is the initial stress), and (4) the weakening rate ($\partial\tau/\partial u$). These effects have important implications for the estimate of the fracture energy as well as for the identification and the meaning of the characteristic SW distance (d_0).

3.3. Behavior of Dynamic Fault Weakening

[15] Figures 4e, 4f, 5e, 5f, 6e, and 6f display the slip-weakening curves and the phase diagrams (i.e., traction versus slip velocity) for different slipping zone thickness, hydraulic diffusivity and the dimensionless parameter α_{LD}, respectively. These simulations clearly demonstrate that thermal pressurization with constant porosity in a relatively thin slipping zone ($w \leq 0.035$ m) or for relatively low values of hydraulic diffusivity ($\omega \leq 0.05$ m^2/s) produces large breakdown stress drop, high slip velocity and large values of the characteristic SW distance (d_0). In particular, we observe from Figures 4f and 5f that the slip velocity can be more than 10 times larger than that inferred for a dry fault. The dimensionless parameter α_{LD} of the *Linker and*

Dieterich [1992] evolution law for the state variable does not change the stress drop and the slip velocities but affects the shape of the slip-weakening curves.

[16] It is important to note that in the RS-dependent friction formulation the characteristic length-scale parameter (L) controlling the state variable evolution is assigned a priori, but not the characteristic SW distance d_0^{eq} [*Cocco and Bizzarri*, 2002; *Bizzarri and Cocco*, 2003]. Our simulations show that thermal pressurization can yield values of the slip-weakening distance much larger than those inferred for a dry fault. Moreover, it is worth noting that for particular configurations the traction evolution displays a gradual and continuous weakening with increasing slip, as proposed by *Abercrombie and Rice* [2005]; for these SW curves the identification of d_0 might be extremely difficult and this parameter might become rather meaningless. This has important implications for the identification of the breakdown zone and the evaluation of its spatial dimension.

4. Variability of Relevant Physical Parameters

[17] The simulations shown thus far demonstrate that thermal pressurization affects the dynamic traction evolution and that the main physical parameters (such as breakdown stress drop, SW distance d_0 and fracture energy) are strongly dependent on the thickness of the slipping zone and the evolution of the effective normal stress. We remind again that only in the framework of RS friction laws the thermally activated pore pressure changes modify both the effective normal stress and the evolution of the friction coefficient (through the state variable evolution). We dis-

cuss in sections 6 and 7 the effects on dynamic traction of using different evolution laws for the state variable as well as including temporal variations of porosity in our calculations. Moreover, the simulations presented in Figures 1–6 have been computed with the set of constitutive parameters listed in Table 1 of BC06. We discuss in this section the slip-weakening curves computed for both SW and DR constitutive laws adopting different sets of constitutive parameters.

[18] Figure 7a shows the traction evolution as a function of slip for three distinct constitutive configurations associated with different values of the strength parameter S. For each configuration we have plotted the slip-weakening curves calculated for dry (solid lines) and wet (dashed lines) conditions. These simulations have been computed for a value of the slipping zone half thickness (w) equal to 1 mm. The solutions computed for $S = 0.8$ have the same model and constitutive parameters listed in Table 1 of BC06 and used in Figures 1–3. The other two (S equal to 1.5 and 1.778, respectively) have different imposed breakdown stress drop (i.e., different values of static and dynamic friction). Figure 7a confirms the results discussed in sections 2 and 3: thermal pressurization with constant porosity is able to increase the breakdown stress drop from 18.0 MPa to 22.9 MPa in the case of $S = 0.8$, from 7.5 MPa to 15.7 MPa for $S = 1.5$ and from 12.5 MPa to 20.3 MPa for $S = 1.778$. We emphasize that in the last two configurations thermal pressurization is able to reduce the effective strength parameter below the critical threshold controlling the transition to supershear rupture velocities.

[19] Figure 7b displays the traction evolution as a function of slip for three different combinations of the a and b constitutive parameters characterizing the DR friction law (values are listed in the legend). Solid curve identifies the solution for a dry configuration, while dashed curves indicate the slip-weakening curves computed for the different constitutive configurations. Figure 7b points out that in the framework of rate- and state-dependent friction, thermal pressurization with constant porosity yields higher values of breakdown stress drop than those computed for dry conditions. Moreover, a comparison between the results shown in Figure 7 suggests that the difference in breakdown stress drop between dry and wet conditions is much larger for a DR law than that inferred for a SW law.

[20] The results obtained in sections 2 and 3 allow the investigation of the scaling relations between the relevant physical parameters discussed above and the slipping zone thickness or the hydraulic diffusivity. These scaling relations might be useful to predict the effect of slipping zone thickness and hydraulic diffusivity on the physical parameters characterizing the dynamic fault weakening. This is discussed in detail in section 5. We emphasize that all the simulations discussed above have been performed under the assumption that the porosity is constant. In other words, it has been assumed that porosity does not evolve with time or that its evolution is slow enough to be negligible during the dynamic rupture propagation. In section 7 we discuss the effects of variable porosity. However, a full exploitation of this problem is beyond the goals of the present study and will be considered in future investigations.

5. Scaling Relations

[21] In sections 2–4 we have discussed the effect of thermal pressurization on dynamic traction evolution and on the main physical parameters controlling the dynamic fault weakening. We have demonstrated that different values of slipping zone thickness and hydraulic diffusivity yield distinct slip-weakening behaviors and different amplitudes of the breakdown stress drop, characteristic SW distance and fracture energy. We summarize these results in this section and we provide scaling relations that associate these physical parameters with the assumed values of slipping zone thickness and hydraulic diffusivity. Figure 8 shows the variations of breakdown stress drop (Figures 8a and 8b), SW distance (d_0, Figures 8c and 8d) and fracture energy (Figures 8e and 8f) as a function of slipping zone half thickness and hydraulic diffusivity (Figures 8a, 8c, and 8e and 8b, 8d, and 8f, respectively). The grey curves show the trend of breakdown stress drop and fracture energy inferred for a SW constitutive law (in this case, d_0 is fixed a priori). The black curves illustrate the scaling of these three parameters retrieved from the simulations performed by adopting RS-dependent friction (DR law stated in equation (2)). The horizontal dotted lines in Figures 8a–8f indicate the values of the physical parameter inferred from simulations performed in dry conditions for both the SW and the DR constitutive formulations. The solid and dashed curves in Figures 8a–8f show the trend inferred from the estimated values and the analytical scaling law, respectively. Figure 8 confirms that the values of these physical parameters characterizing the dynamic traction evolution are different from those evaluated from simulations performed in dry conditions. This means that thermal pressurization and frictional heating modify the dynamic fault weakening, at least in the range of slipping zone thickness and hydraulic diffusivity values investigated in this study and for a constant porosity model.

[22] Figure 8 reveals that the variations of breakdown stress drop and fracture energy caused by thermal pressurization with constant porosity in a fault model governed by a SW law are much smaller than those produced by a DR friction law. This is also evident from the results shown in Figure 7. For the particular set of constitutive parameters

Figure 8. Dependencies of the physical observables on the thermal pressurization parameters w (Figures 8a, 8c, and 8e) and ω (Figures 8b, 8d, and 8f). (a) and (b) Breakdown stress drop. (c) and (d) Equivalent characteristic SW distance in the case of DR numerical experiments. The ratio between the modeled d_0^{eq} and the characteristic length L is reported in both panels. (e) and (f) Fracture energy. In all plots, gray curves refer to slip-weakening simulations, while black curves refer to the Dieterich-Ruina simulations; dotted lines indicate the value obtained in dry conditions. In Figures 8a, 8b, 8c, and 8d, dashed lines represent the proposed scaling relations (see text for details), while in Figures 8e and 8f they indicate the fracture energy in the SW cases calculated using the linear relation $E_G = \Delta\tau_b/2d_0$ instead of the numerical integration (equation (1)).
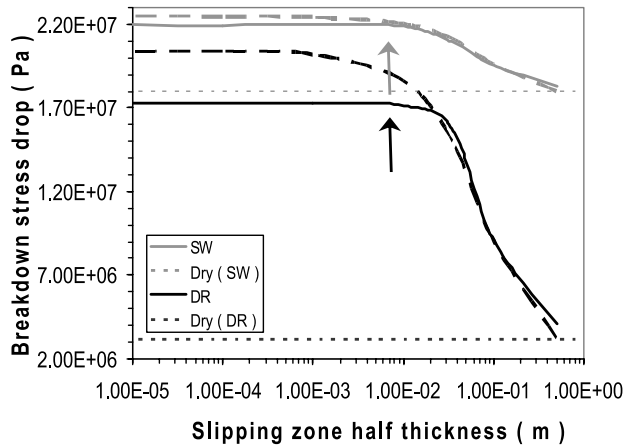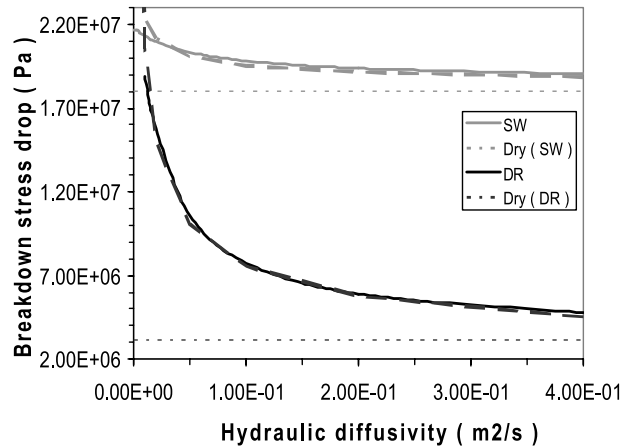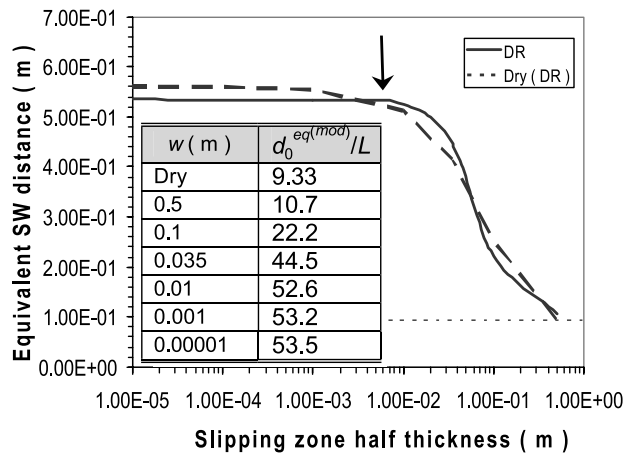
Figure 8

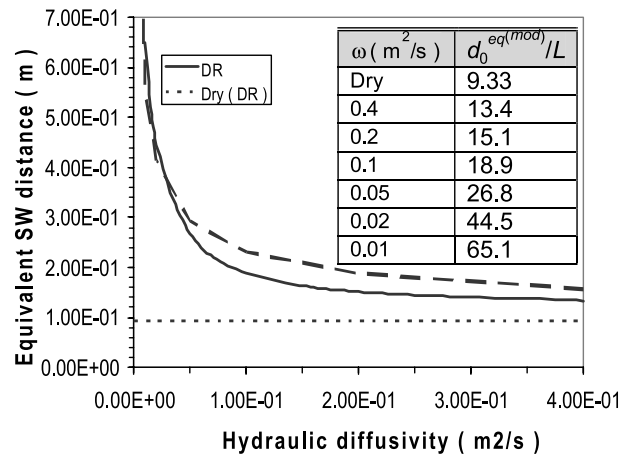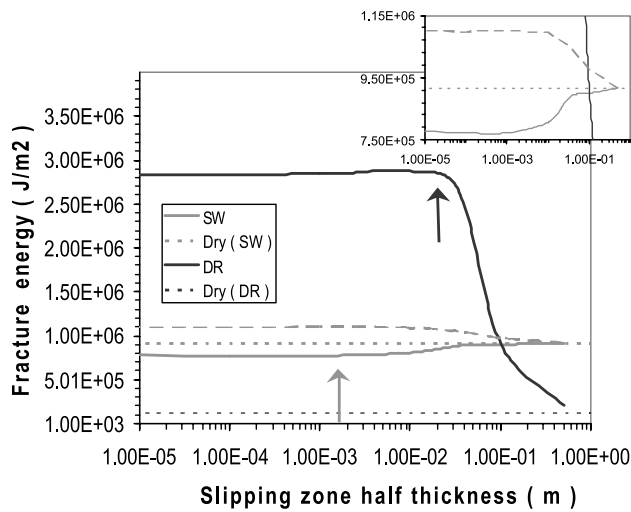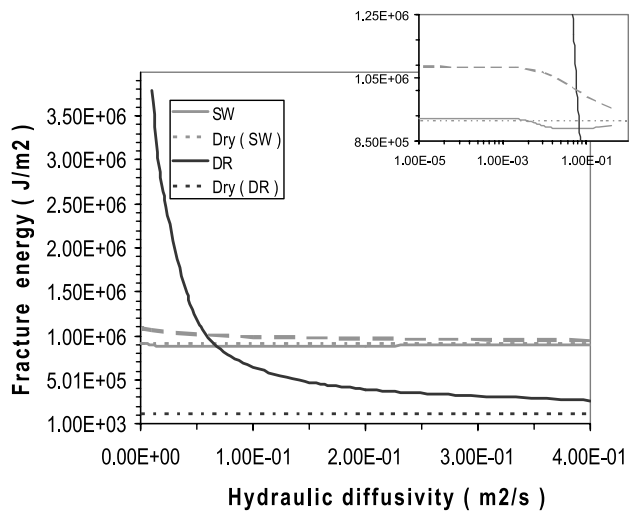used in Figure 8 for the SW law, the difference between values of breakdown stress drop for wet and dry faults is nearly 27%. However, the increase of breakdown stress drop for wet faults governed by a SW law can be larger when the initial difference between static and dynamic friction coefficients is smaller (as shown in Figure 7 for $S = 1.5$). This dependence on the initial values of friction coefficients is due to the fact that adopting a SW constitutive law, the characteristic SW distance (d_0) and the initial shape of the slip weakening curve are prescribed a priori. Thus thermal pressurization can only reduce the residual stress level and modify the weakening rate. This explains why, for particular constitutive configurations the fracture energy estimated for a wet fault governed by a SW law can be slightly smaller than the value associated with the dry fault.

[23] Figures 7 and 8 point out that the alternative choice of a RS-dependent friction law yields large variations of the main physical parameters and relevant differences with respect to the values obtained from dry conditions. We therefore focus our attention on the simulations performed with RS friction.

[24] A general inspection of the results shown in Figure 8 points out that (1) breakdown stress drop, SW distance and fracture energy continuously decrease as a function of the hydraulic diffusivity, (2) these parameters display a different behavior as a function of the slipping zone thickness, being nearly constant with a sudden drop after a given threshold value (indicated by an arrow in Figure 8), and (3) thermal pressurization can yield values of fracture energy consistent with seismological estimates ($\sim 10^6$ J/m^2) also when constitutive parameters a and b have values derived from laboratory experiments and L is scaled to real fault dimension from laboratory derived values. The latter result has important implications for bridging laboratory and real fault estimates of fracture energy [*McGarr et al.*, 2004].

[25] The trend shown by our estimated values is well described by the following analytical scaling relations:

$$\Delta\tau_b = \Delta\tau_b^{(\mathrm{dry})}\left(1 + a_2 e^{-\frac{w}{d}}\right)\left(a_3 + a_4\sqrt{\frac{\omega*}{\omega}}\right) \qquad (4)$$

for the breakdown stress drop (Figures 8a and 8b) and

$$d_0^{eq} = d_0^{eq(\mathrm{dry})}\left(1 + b_2 e^{-\frac{w}{d}}\right)\left(b_3 + b_4\sqrt{\frac{\omega*}{\omega}}\right) \qquad (5)$$

for the equivalent characteristic SW distance in the DR simulations (Figures 8c and 8d). The values of the parameters appearing in (4) are, for the SW law: $a_2 = 0.25$, $a_3 = 0.86$, $a_4 = 0.14$, $d = d_0^{(\mathrm{dry})}$, while for the RS law $a_2 = 5.5$, $a_3 = 0.1$, $a_4 = 0.9$, $d = d_0^{eq(\mathrm{dry})}$. The scaling relation (5) holds for a RS constitutive law and the parameters are $b_2 = 5$, $b_3 = 0.2$, $b_4 = 0.8$; d is the equivalent characteristic SW distance ($d_0^{eq(\mathrm{dry})}$). In both previous equations $\omega*$ is equal to 0.02 m^2/s. These analytical relations are plotted as dashed lines in Figures 8b, 8c, and 8d. It is clear from equations (4) and (5) that for high w and ω the predicted values of breakdown stress drop and equivalent characteristic SW distance approach the dry limit.

[26] Our simulations and inferred scaling relations indicate that the breakdown stress drop, characteristic SW distance and the fracture energy are nearly constant and independent of the slipping zone thickness for w smaller than 0.02 m (as indicated by the arrows in Figure 8). This range represents relatively thin slipping zones. In these conditions thermal pressurization with constant porosity can be very important, because the physical parameters differ substantially from the corresponding values obtained in the dry configuration. As expected, for high values of w and ω they approach the dry configuration (indicated by the dotted horizontal lines in Figure 8). We emphasize that for the DR case, the ratio of the numerically modeled d_0^{eq} to the imposed L is not constant. In the reference dry case this ratio is nearly 10, in agreement with *Cocco and Bizzarri* [2002] and *Bizzarri and Cocco* [2003]. However, when thermal pressurization becomes relevant, d_0^{eq} can grow becoming higher than 60. This implies that in these models the characteristic SW distance can reach 0.5 m (or even greater), in agreement with seismological estimates [see *Dalguer et al.*, 2002; *Tinti et al.*, 2004].

## 6. Importance of State Variable Evolution

[27] In this section we aim to compare the pore pressure and dynamic traction evolution inferred by solving the thermal pressurization problem with constant porosity using the two different evolution laws defined in equations (2) and (3). These two formulations of RS-dependent friction differ only for the evolution of the state variable: we remind here that in this study we name DR (Dieterich-Ruina) the aging constitutive law defined in (2) and RD (Ruina-Dieterich) that defined in (3). It is important to emphasize that in a thermal pressurization model aimed to represent the breakdown processes occurring within a slipping zone of finite thickness the meaning of the state variable should be different with respect to that proposed in the original formulation of RS friction. A discussion on the interpretation of the state variable is beyond the goals of this study and we rely on the interpretations of *Sleep* [1997], who also considers the main physical quantities as macroscopic averages.

[28] We display the results of our simulations in Figure 9. Figure 9b shows the state variable behavior for the DR and RD friction laws; although they have the same initial and final steady state values, their temporal evolutions are very different. In particular, the RD law exhibits a very fast drop to the final value and it does not evolve far away from the steady state. On the contrary, the DR law has a peculiar evolution with an evident increase (see the bump in Figure 9b) before its drop to the final steady state. In order to have an increase from its initial value, the time derivative of the state variable must become positive. Depending on the values of the parameters and the combination of slip velocity and effective normal stress, for the DR law $\dot{\Psi} > 0$ occurs if, and only if, the following equation is satisfied:

$$\frac{\alpha_{\mathrm{LD}}|\dot{\sigma}_n^{\mathrm{eff}}|}{b\sigma_n^{\mathrm{eff}}} > \frac{v}{L} - \frac{1}{\Psi}. \qquad (6)$$
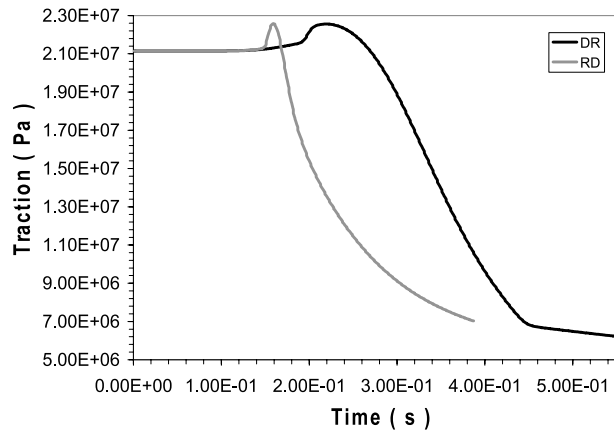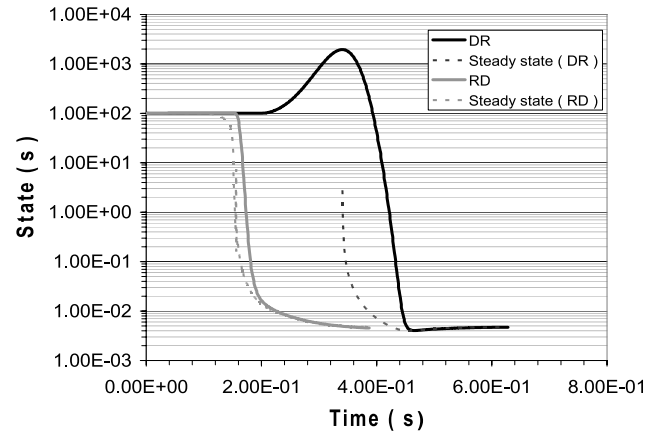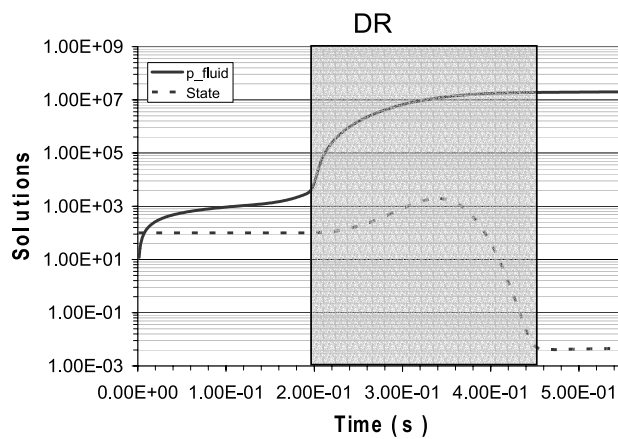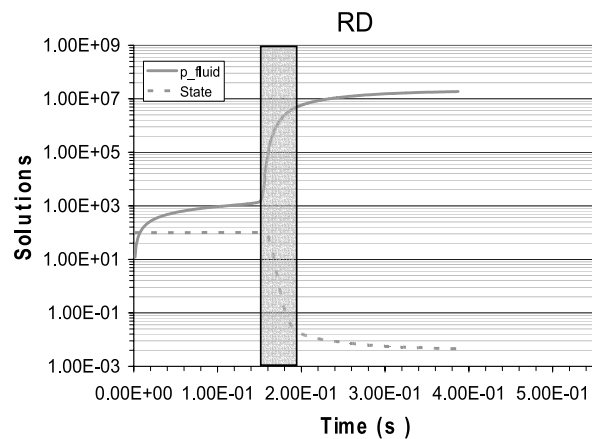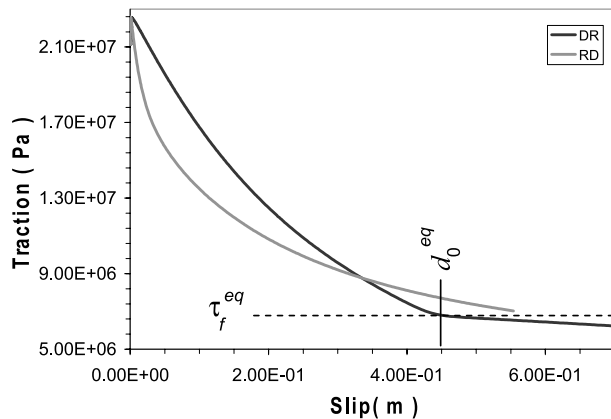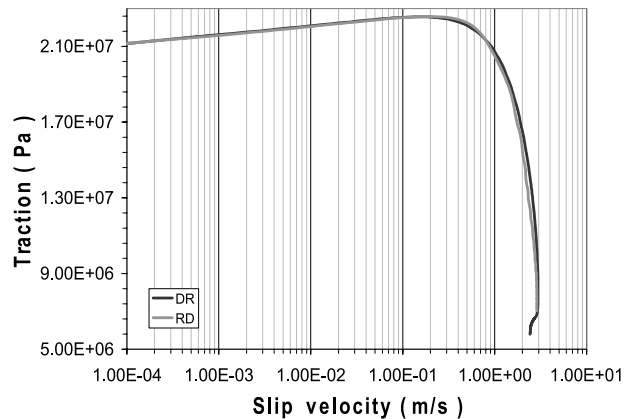
Figure 9. Comparison between simulations performed with the Dieterich-Ruina (DR, black curves) and Ruina-Dieterich (RD, gray curves) governing equations for a wet fault. (a) and (b) Time evolutions of the fault friction and state variable. (c) and (d) Superposition of state variable and fluid pressure time evolutions for the DR and the RD constitutive formulations, respectively. (e) Slip-weakening curves and (f) the phase diagram for both solutions. All parameters are the same for the two constitutive laws (see Table 1 of BC06) and the fault point is the same of Figures 4 to 6.

[29] On the contrary, the RD law always displays a negative time derivative of the state variable, as the following equations is never satisfied:

$$\frac{\alpha_{LD} \left| \dot{\sigma}_n^{eff} \right|}{b\sigma_n^{eff}} > \frac{v}{L} \ln\left(\frac{v\Psi}{L}\right) \quad (7)$$

[30] Figures 9c and 9d allow the comparison between state variable and pore fluid pressure evolutions; pore fluid pressure changes inferred for the two constitutive formulations are similar, but the RD law yields faster pore fluid pressure changes. It is worth noting that the state variable increase in the DR law occurs later than the pore pressure raise, the latter being determined by temperature changes. We observe that the final level of the friction is nearly the same (Figures 9a and 9e), as well as the slip velocity (Figure 9f). This is due to the fact that the final values of pore fluid pressure are nearly the same, as well as the final value of the state variable (Figures 9c and 9d). It is interesting to notice that also for the wet RD law, the state variable is at the steady state at the end of the breakdown process (Figure 9b).

[31] The comparison presented in Figure 9 reveals that the shape of the slip-weakening curve (displayed in Figure 9e) is modified by the state variable evolution. In particular, thermal pressurization in a fault zone governed by a RD friction law yields a slip-weakening curve displaying a continuous decrease without a clear residual stress level that would allow the measurement of the characteristic slip-weakening distance. On the contrary, although the slip-weakening curve inferred for the DR law also shows a nearly continuous decrease, it still allows the determination of the equivalent characteristic slip-weakening distance and of a slowly variable residual stress level.

7. Effects of Porosity Evolution

[32] In all the numerical experiments presented and discussed up to now we assumed that the porosity Φ was constant over time and the variations of hydraulic diffusivity are obtained through changing the permeability. The solution of such a simplified thermal pressurization model is presented in BC06 (BC06, equation (9) and Appendix B). We consider now a model in which the porosity may evolve with time within the breakdown time duration. The solution of the generalized thermal pressurization problem with variable porosity is presented in Appendix A.

[33] In the literature several analytical relations have been proposed to represent the evolution of Φ [see, e.g., *Nakatani*, 1998; *Segall and Rice*, 1995; *Sleep*, 1995a, 1995b, 1997, 1999]. In this paper we assume that the porosity varies according to the model proposed by *Segall and Rice* [1995]; in particular, we assume that it is related to the state variable evolution through the following law:

$$\Phi(\xi_1, \zeta, \xi_3, t) = \Phi_* - \varepsilon_{SR} \ln\left(\frac{\Psi v_*}{L_{SR}}\right) \quad (8)$$

where Φ_* is the reference value for the porosity, assumed to be homogeneous over the slipping zone thickness; ε_{SR} and L_{SR} are two parameters representing the sensitivity to the state variable evolution and a length scale, respectively. We choose Φ_* in order to have at the beginning of the simulations ($t = 0$) a porosity value equal to the that adopted in previous numerical experiments with constant porosity ($\Phi = 0.025$). The values of the other two constitutive parameters are listed in Table 1 of BC06. We point out that equation (8) includes a length parameter (L_{SR}) that in general may be different from the length parameter (L) used in the RS friction laws (see equations (2) and (3)). In the simulations presented in the following we assume that the two length scales are identical, in agreement with *Segall and Rice* [1995]. Nevertheless, we have verified that at least within the timescales of dynamic fault weakening, there are no appreciable differences in solutions obtained with different values of L_{SR}.

[34] In Figure 10 we plot the results of a numerical simulation performed adopting the DR law (equation (3)) with the pore fluid pressure variation expressed by (A5). We observe that the inferred slip velocity evolution does not change, with some differences at high slip rates. The evolution of the state variable is also slightly modified (see Figure 10b). On the contrary, the pore pressure change obtained with variable porosity is quite different from that inferred for a constant porosity model (see Figure 10d): the constant porosity model (black curve) yields fluid pressure which continuously increases with time, while pore pressure for the variable porosity model (gray curve) shows two clear change episodes. The second perturbation is due to the second term in the integrand of (A5), which represents a competing effect on pore fluid evolution caused by the heating term ($\tau(\xi_1, \xi_3, t')v(\xi_1, \xi_3, t')$). Figure 10d clearly shows that the temporal evolution of porosity reduces the pore pressure changes with respect to a constant porosity model, as expected from equation (A5). Conversely, the slip-weakening curve is slightly changed (see Figure 10c); yield and final stress values are unaffected, but the shape of the curve is modified. A variable porosity model yields a gradual and continuous dynamic weakening more similar to a power law [see *Abercrombie and Rice*, 2005], without a clear characteristic SW distance.

8. Discussion

[35] Our numerical experiments confirm the findings of previous investigations that thermal pressurization plays an important role in earthquake dynamic ruptures [e.g., *Sibson*, 1977; *Kanamori and Heaton*, 2000; *Andrews*, 2002; *Fialko*, 2004]. The results presented in this and in BC06 shed light on the effects of frictional heating and thermal pressurization on the dynamic traction evolution and earthquake rupture propagation. We have addressed the particular problem of the propagation of a dynamic rupture governed by different constitutive laws and we have investigated how thermal pressurization can alter the dynamic traction during this coseismic phase (i.e., the dynamic fault weakening). *Kanamori and Heaton* [2000] suggested that the temperature changes caused by frictional sliding depend on the thickness of the slipping zone and on the earthquake magnitude. These authors concluded that because thermal processes are important only for large earthquakes, the dynamics of small and large earthquakes can be very different. Our simulation strategy is based on the assump-
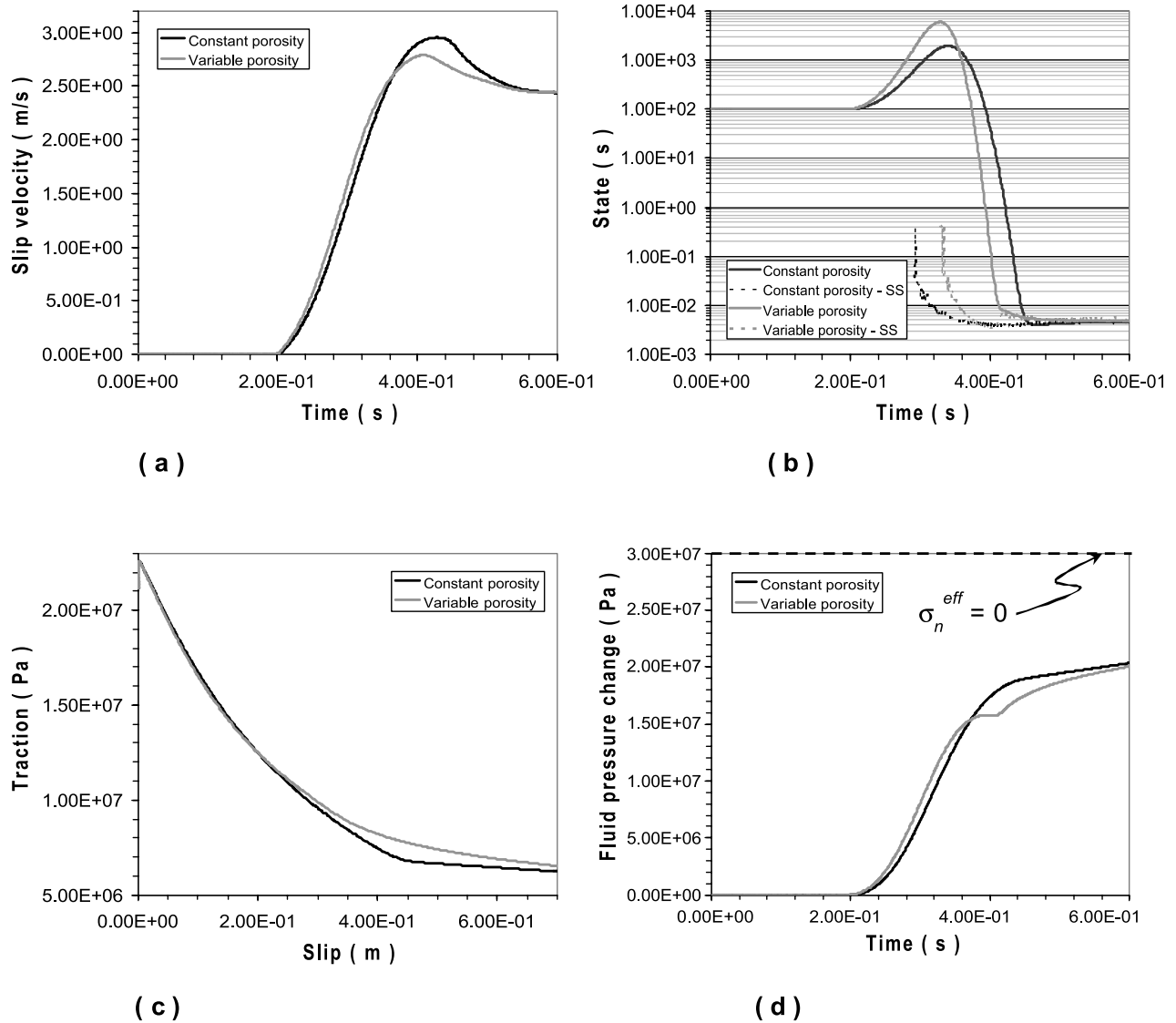
Figure 10. Comparison between simulation adopting the Dieterich-Ruina law for wet configurations. The black curves refer to the reference case with constant porosity, while gray curves refer to case in which the porosity varies during time, according to the *Segall and Rice* [1995] model. (a) Fault slip velocity evolution. (b) State evolution, with the superposition of the steady state curves (Ψ^{ss} is indicated by dashed lines). (c) Slip-weakening diagrams. (d) Fluid pressure change evolution. All the parameters are listed in Table 1 of BC06.

tion that rate- and state-dependent friction controls the weakening process for small slip amplitudes and that additional thermal weakening would contribute and dominate, in some configurations, at large slips (see traction evolutions in Figures 4 and 5). Therefore the question is if small earthquakes can experience thermal pressurization. On the basis of the relatively low radiated energy of small earthquakes, *Kanamori and Heaton* [2000] and *Abercrombie and Rice* [2005] suggest that small earthquakes should never undergo thermal weakening by fluid pressurization.

[36] The results of the present study confirm that an earthquake rupture in a relatively thin slipping zone ($w \leq$ 1 mm) yields temperature changes large enough to produce melting ($\Delta T \geq 1000°C$). We have also shown that even if fluids are present in the fault zone and in the surroundings,

the decrease in temperature perturbations caused by thermal pressurization may not be enough to prevent melting. In other words, for extremely localized slip the temperature increase caused by frictional heating and thermal pressurization might still be relatively large ($\Delta T \cong 800°C$). Our calculations corroborate that temperature changes depend on the slip amplitude; the larger the slip the larger the temperature increase (see Figure 6a of BC06). However, it is important to point out that our temperature change calculations are not computed for adiabatic conditions; we solve the 1-D heat conduction problem considering appropriate heat sources within the slipping zone (see BC06). In this context, the dependence of the calculated temperature perturbations on slip amplitude is not linear as in adiabatic conditions. Although our numerical results do not contradict

the *Kanamori and Heaton* [2000] conclusion concerning the different temperature changes associated with large and small earthquake (that is, small and large slip amplitudes), our simulations suggest that the effects of the slipping zone thickness on the temperature changes are more significant than the slip amplitude. In other words, the temperature changes in an extremely thin fault ($w \leq 1$ mm) associated with slip episodes larger than 0.05 m do not differ considerably from those associated with 1 m of slip. This suggests that the temperature dependence on slip might not be enough to explain the difference between seismic energy of small and large earthquakes.

[37] Another interesting implication of our numerical experiments is that in the case of RS governing laws, the equivalent characteristic SW distance and the fracture energy increase with the distance from the nucleation patch. This result is consistent with several previous investigations [*Andrews*, 1976; *Scholz et al.*, 1993]. The scaling of fracture energy with the rupture length is expected, since our results are consistent with crack-like solutions rather than self-healing pulses. However, the finding that the equivalent characteristic SW distance (d_0^{eq}) can assume amplitudes relatively larger than those expected in dry conditions has important implications for the earthquake energy budget [see *Abercrombie and Rice*, 2005, and references therein]. In other words, thermal pressurization contributes in growing d_0^{eq}, which can become for extremely thin slipping zone a significant fraction of total slip. It is likely that in these cases the SW distance can be larger than average slip in small earthquakes, supporting the interpretation that d_0^{eq} is a scale-dependent parameter.

[38] Finally, we point out that the shape of the SW curve depends on the thickness of the slipping zone and the hydraulic diffusivity value, but it is also modified by the contribution of effective normal stress changes included in the *Linker and Dieterich* [1992] evolution law. In particular, the adopted evolution law strongly controls the shape of the slip-weakening curves. Results from simulations performed for variable porosity, governed by an appropriate evolution law [*Segall and Rice*, 1995], reveal that dynamic weakening is modified by the state variable evolution. In particular configurations we have found that the slip-weakening curves are characterized by a gradual and continuous decrease in traction resembling an exponential or a power law [see *Abercrombie and Rice*, 2005]. This particular shape makes it difficult to compute fracture energy, to evaluate the size of the breakdown zone as well as to separate the local contribution of frictional heating and surface energy [see *Abercrombie and Rice*, 2005; *Tinti et al.*, 2005, and references therein] because it is impossible to identify a minimum residual stress level and the characteristic SW distance. However, we remind that in the framework of frictional heating investigated in this study, it has been implicitly assumed that all the work is converted into heat. We call attention to the inferred values of fracture energy resulting from the simulations performed in this study that are in agreement with seismological estimates of fracture energy ($\sim 10^6$ J/m²).

[39] The results of this study emphasize that thermal pressurization increases the breakdown stress drop with respect to the values expected in dry conditions. This stress drop increase is quite large, suggesting that thermal pres-

surization can produce a nearly complete stress drop. This conclusion raises an interesting question: If the results of these numerical simulations are applicable to real earthquakes, we should find a signature of these high stress drop values in the radiated seismograms. Seismological estimates of stress drop do not support the common evidence of a nearly complete stress release during dynamic failure. Therefore we have two possible explanations: the estimation of stress drop from seismic waves is biased (for instance by the difficulties in analyzing high frequency radiation) or the effects of thermal pressurization on the dynamic traction evolution are less pronounced than those predicted by a constant porosity model. This might be the case, if the thickness of the slipping zone is relatively large ($w > 50$ mm, for instance), however geological observations [see *Sibson*, 2003, and references therein] do not support this finding. We do not aim to answer to this question in this study. We only point out that the role of porosity and permeability variations during the rupture propagation has to be better taken into account to model earthquake ruptures and to understand dynamic fault weakening.

9. Conclusions

[40] In this and in BC06 we have investigated the role of thermal pressurization on the dynamic rupture propagation of a spontaneous truly 3-D rupture in a homogeneous half-space. In particular, in BC06 we have shown that thermal pressurization affects the shape and the propagation velocity of the rupture front on the assumed fault plane. Our simulations reveal that the thickness of the slipping zone plays a relevant role in controlling the dynamic traction evolution within the cohesive zone. We have performed in this study many different numerical experiments to understand the role of slipping zone thickness and hydraulic diffusivity value on temporal variation of friction coefficient and effective normal stress. We can conclude that thermal pressurization increases the breakdown stress drop, the peak slip velocity and consequently the inferred fracture energy. The latter also depends on the characteristic slip-weakening distance d_0^{eq} [see *Bizzarri and Cocco*, 2003, and references therein]: we have shown that thermal pressurization increases the SW distance up to half of a meter (for a reference d_0^{eq} value in dry conditions of the order of 10 mm). We propose scaling relations to evaluate the effects of slipping zone thickness and hydraulic diffusivity on breakdown stress drop and the characteristic slip-weakening distance. The analytical dependence on hydraulic diffusivity included in the scaling law and retrieved in this study agrees with the results of *Andrews* [2002].

[41] Moreover, in the framework of rate- and state-dependent friction laws, our results suggest that thermal pressurization and the state variable evolution (which in this case depends on the effective normal stress and/or porosity) modify the traction evolution and can yield slip-weakening curves characterized by a gradual and continuous decrease in traction [see *Abercrombie and Rice*, 2005]. In this case the definitions of a minimum residual stress level and the characteristic slip-weakening distance become meaningless.

[42] Most of the simulations in this study have been performed for a constant porosity. Each numerical experi-

ments has been performed by assuming that elastodynamics governs off fault materials and permeability is constant throughout the medium. *Wibberley and Shimamoto* [2003] provided evidence that permeability values can change in the direction normal to the fault plane. In this study we have also considered the effect of porosity evolution, although a complete investigation of the effects of temporal variations of porosity is beyond the goals of this study. Our simulations confirm that porosity evolution can modify dynamic traction. If the porosity and permeability are sufficiently high during the dynamic rupture propagation, little or no pressurization can occur. This is because temporal porosity changes can counterbalance the contribution of frictional heating and fluid flow in determining pore pressure temporal evolution. We point out that pore pressure modifies the state variable evolution and therefore affects the shape of the slip-weakening curve. Further research is needed to measure permeability and porosity variations in fault zones and to constrain their temporal and spatial variations.

Appendix A: Solution of the Generalized Thermal Pressurization Problem

[43] In Appendix B of BC06 we have derived the solution of the 1-D thermal pressurization problem under the hypothesis of constant porosity. In general the porosity Φ can change in time, accordingly to an evolution law, that has to be assigned a priori. If porosity changes, we have to consider the generalized problem described by the coupled equations (5) and (7) of BC06. In this case the hydraulic diffusivity ω is also varying in time, as it explicitly depends on porosity (see equation (8) of BC06). In the following, we assume for simplicity that parameters $\gamma \equiv \alpha_{\text{fluid}}/(\beta_{\text{fluid}}c)$ and β_{fluid}, porosity and its time derivative are constant in space and do not vary within the slipping zone.

[44] If we calculate the partial time derivative of temperature T from equation (5) of BC06 and we insert this expression in equation (B6) of BC06, describing the simplified thermal pressurization problem, we obtain:

$$\frac{\partial}{\partial t}p_{\text{fluid}} - \frac{\alpha_{\text{fluid}}}{\beta_{\text{fluid}}}\chi\frac{\partial^2}{\partial\zeta^2}T - \omega\frac{\partial^2}{\partial\zeta^2}p_{\text{fluid}} = \frac{\alpha_{\text{fluid}}}{\beta_{\text{fluid}}}\frac{1}{c}q, \qquad (A1)$$

where β_{fluid} is the coefficient of the compressibility of the fluid and α_{fluid} is the coefficient of thermal expansion of the fluid, χ is the thermal diffusivity, c is the heat capacity for unit volume of the bulk composite, q is the heat generated for unit volume and for unit time and ζ is the spatial coordinate normal to the fault (see Figure 1b of BC06).

[45] Moreover, if we calculate $\partial T/\partial t$ from equation (5) of BC06 and we insert this expression in equation (7) of BC06, that defines the generalized thermal pressurization problem, we have:

$$\frac{\partial}{\partial t}p_{\text{fluid}} - \frac{\alpha_{\text{fluid}}}{\beta_{\text{fluid}}}\chi\frac{\partial^2}{\partial\zeta^2}T - \omega\frac{\partial^2}{\partial\zeta^2}p_{\text{fluid}} = \frac{\alpha_{\text{fluid}}}{\beta_{\text{fluid}}}\frac{1}{c}q - \frac{1}{\beta_{\text{fluid}}\Phi}\frac{\partial}{\partial t}\Phi$$
$$(A2)$$

[46] The comparison between (A1) and (A2) suggests that the solution of the fluid pressure $\tilde{p}_{\text{fluid}}$ for the generalized thermal pressurization problem can be obtained in the same way as Appendix B of BC06, except for calculating the time convolution and the integral over the normal coordinate ζ of the Green's kernel $p_{\text{fluid}}^{el}(\zeta, t)$ of equation (B7) of BC06 using the following term as the actual heat source

$$\tilde{q}(\xi_1, \zeta, \xi_3, t)$$
$$= \begin{cases} \dfrac{\tau(\xi_1,\xi_3,t)v(\xi_1,\xi_3,t)}{2w(\xi_1,\xi_3)} - \dfrac{1}{\gamma\beta_{\text{fluid}}\Phi}\dfrac{\partial}{\partial t}\Phi & , t > 0, |\zeta| \leq w(\xi_1,\xi_3) \\[1em] 0 & , |\zeta| > w(\xi_1,\xi_3) \end{cases}$$
$$(A3)$$

instead of $q(\xi_1, \zeta, \xi_3, t)$ of equation (A2) of BC06. Simple algebra shows that:

$$\tilde{p}_{\text{fluid}}^w(\xi_1, \zeta, \xi_3, t) = p_{\text{fluid}_0} + \frac{\gamma}{4w(\xi_1,\xi_3)}\int_0^{t-\varepsilon} d\,t'$$

$$\cdot\left\{-\frac{\chi}{\omega-\chi}\left[\text{erf}\left(\frac{\zeta+w(\xi_1,\xi_3)}{2\sqrt{\chi(t-t')}}\right) - \text{erf}\left(\frac{\zeta-w(\xi_1,\xi_3)}{2\sqrt{\chi(t-t')}}\right)\right]\right.$$
$$\left.+\frac{\omega}{\omega-\chi}\left[\text{erf}\left(\frac{\zeta+w(\xi_1,\xi_3)}{2\sqrt{\omega(t-t')}}\right) - \text{erf}\left(\frac{\zeta-w(\xi_1,\xi_3)}{2\sqrt{\omega(t-t')}}\right)\right]\right\}$$
$$\cdot\left\{\tau(\xi_1,\xi_3,t')v(\xi_1,\xi_3,t') - \frac{2w(\xi_1,\xi_3)}{\gamma}\right.$$
$$\left.\cdot\frac{1}{\beta_{\text{fluid}}\Phi(t')}\frac{\partial}{\partial t'}\Phi(\xi_1,\zeta,\xi_3,t')\right\}$$
$$(A4)$$

where $p_{\text{fluid}_0} \equiv p_{\text{fluid}}(\xi_1, \zeta, \xi_3, 0)$, as in Appendix B of BC06, erf( ) is the error function

$$\left(\text{erf}(z)\underset{df}{=}\frac{2}{\sqrt{\pi}}\int_0^z dx e^{-x^2}\right)$$

and ε is an arbitrarily small positive real number.

[47] On the fault plane (i.e., in the limit of $\zeta \to 0$) the analytical solution for the fluid pressure is:

$$\tilde{p}_{\text{fluid}}^{w^f}(\xi_1, \xi_3, t) = p_{\text{fluid}_0}^f + \frac{\gamma}{2w(\xi_1,\xi_3)}\int_0^{t-\varepsilon} dt'$$

$$\cdot\left\{-\frac{\chi}{\omega-\chi}\text{erf}\left(\frac{w(\xi_1,\xi_3)}{2\sqrt{\chi(t-t')}}\right)\right.$$
$$\left.+\frac{\omega}{\omega-\chi}\text{erf}\left(\frac{w(\xi_1,\xi_3)}{2\sqrt{\omega(t-t')}}\right)\right\}$$
$$\cdot\left\{\tau(\xi_1,\xi_3,t')v(\xi_1,\xi_3,t')\right.$$
$$\left.-\frac{2w(\xi_1,\xi_3)}{\gamma}\frac{1}{\beta_{\text{fluid}}\Phi(t')}\frac{\partial}{\partial t'}\Phi(\xi_1,0,\xi_3,t')\right\} \quad (A5)$$

where $p_{\text{fluid}_0}^f \equiv p_{\text{fluid}}(\xi_1,0,\xi_3,0)$, as in Appendix B of BC06. Let us emphasize that in equations (A4) and (A5) the hydraulic diffusivity implicitly depends on time. Moreover, for constant porosity (i.e., $\Phi(\xi_1, \zeta, \xi_3, t) = \Phi_0(\xi_1, \zeta, \xi_3)$) solutions (A4) and (A5) become, as expected, the solutions

derived in equations (B8) and (B9) of Appendix B of BC06, respectively, for the simplified thermal pressurization problem of the pore fluid.

References

Abercrombie, R. E., and J. R. Rice (2005), Can observations of earthquake scaling constrain slip weakening?, *Geophys. J. Int.*, *162*, 406–424.

Andrews, D. J. (1976), Rupture propagation with finite stress in antiplane strain, *J. Geophys. Res.*, *81*, 3575–3582.

Andrews, D. J. (2002), A fault constitutive relation accounting for thermal pressurization of pore fluid, *J. Geophys. Res.*, *107*(B12), 2363, doi:10.1029/2002JB001942.

Beeler, N. M., T. E. Tullis, and J. D. Weeks (1994), The roles of time and displacement in the evolution effect in rock friction, *Geophys. Res. Lett.*, *21*, 1987–1990.

Bizzarri, A., and M. Cocco (2003), Slip-weakening behavior during the propagation of dynamic ruptures obeying rate- and state-dependent friction laws, *J. Geophys. Res.*, *108*(B8), 2373, doi:10.1029/2002JB002198.

Bizzarri, A., and M. Cocco (2005), 3-D dynamic simulations of spontaneous rupture propagation governed by different constitutive laws with oblique initial stress direction, *Ann. Geophys.*, *48*, 277–299.

Bizzarri, A., and M. Cocco (2006), A thermal pressurization model for the spontaneous dynamic rupture propagation on a three-dimensional fault: 1. Methodological approach, *J. Geophys. Res.*, *111*, B05303, doi:10.1029/2005JB003862.

Campillo, M., and I. R. Ionescu (1997), Initiation of antiplane shear instability under slip dependent friction, *J. Geophys. Res.*, *102*, 20,363–20,371.

Cocco, M., and A. Bizzarri (2002), On the slip-weakening behavior of rate-and state dependent constitutive laws, *Geophys. Res. Lett.*, *29*(11), 1516, doi:10.1029/2001GL013999.

Dalguer, L. A., K. Irikura, W. Zhang, and J. D. Riera (2002), Distribution of dynamic and static stress changes during 2000 Tottori (Japan) earthquake: Brief interpretation of the earthquake sequences; foreshocks, mainshock and aftershocks, *Geophys. Res. Lett.*, *29*(16), 1758, doi:10.1029/2001GL014333.

Das, S., and K. Aki (1977a), A numerical study of two-dimensional spontaneous rupture propagation, *Geophys. J. R. Astron. Soc.*, *50*, 643–668.

Das, S., and K. Aki (1977b), Fault plane with barriers: A versatile earthquake model, *J. Geophys. Res.*, *82*, 5658–5670.

Fialko, Y. (2004), Temperature fields generated by the elastodynamic propagation of shear cracks in the Earth, *J. Geophys. Res.*, *109*, B01303, doi:10.1029/2003JB002497.

Kanamori, H., and T. H. Heaton (2000), Microscopic and macroscopic physics of earthquakes, *GeoComplexity and the Physics of Earthquakes*, *Geophys. Monogr. Ser.*, vol. 120, edited by J. B. Rundle, D. L. Turcotte, and W. Klein, pp. 147–163, AGU, Washington, D. C.

Lachenbruch, A. H. (1980), Frictional heating, fluid pressure, and the resistance to fault motion, *J. Geophys. Res.*, *85*, 6097–6122.

Linker, M. F., and J. H. Dieterich (1992), Effects of variable normal stress on rock friction: Observations and constitutive equations, *J. Geophys. Res.*, *97*, 4923–4940.

Mair, K., and C. Marone (1999), Friction of simulated fault gauge for a wide range of slip velocities and normal stresses, *J. Geophys. Res.*, *104*, 28,899–28,914.

Manning, C. E., and S. E. Ingebritsen (1999), Permeability of the continental crust: Implications of geothermal data and metamorphic systems, *Rev. Geophys.*, *37*, 127–150.

McGarr, A., J. B. Fletcher, and N. M. Beeler (2004), Attempting to bridge the gap between laboratory and seismic estimates of fracture energy, *Geophys. Res. Lett.*, *31*, L14606, doi:10.1029/2004GL020091.

Miller, S. A. (2002), Properties of large ruptures and the dynamical influence of fluids on earthquakes and faulting, *J. Geophys. Res.*, *107*(B9), 2182, doi:10.1029/2000JB000032.

Nakatani, M. (1998), A new mechanism of slip weakening and strength recovery of friction associated with the mechanical consolidation of gouge, *J. Geophys. Res.*, *103*, 27,239–27,256.

Noda, H., and T. Shimamoto (2005), Thermal pressurization and slip-weakening distance of a fault: An example of the Hanaore Fault, Southwest Japan, *Bull. Seismol. Soc. Am.*, *95*(4), 1224–1233, doi:10.1785/0120040089.

Ohnaka, M. (2003), A constitutive scaling law and a unified comprehension for frictional slip failure, shear fracture of intact rock, and earthquake rupture, *J. Geophys. Res.*, *108*(B2), 2080, doi:10.1029/2000JB000123.

Ohnaka, M., Y. Kuwahara, and K. Yamamoto (1987), Constitutive relations between dynamic physical parameters near a tip of the propagating slip zone during stick-slip shear failure, *Tectonophysics*, *144*, 109–125.

Okubo, P. G., and J. H. Dieterich (1984), Effects of physical fault properties on frictional instabilities produced on simulated faults, *J. Geophys. Res.*, *89*, 5817–5827.

Palmer, A. C., and J. R. Rice (1973), The growth of slip surfaces in the progressive failure of overconsolidated clay, *Proc. R. Soc. London, Ser. A*, *332*, 527–548.

Scholz, C. H., N. H. Dawers, J.-Z. Yu, M. H. Anders, and P. A. Cowie (1993), Fault growth and fault scaling laws: Preliminary results, *J. Geophys. Res.*, *98*, 21,951–21,961.

Segall, P., and J. R. Rice (1995), Dilatancy, compaction, and slip instability of a fluid-infiltrated fault, *J. Geophys. Res.*, *100*, 22,155–22,171.

Sibson, R. H. (1977), Kinetic shear resistance, fluid pressures and radiation efficiency during seismic faulting, *Pure Appl. Geophys.*, *115*, 387–400.

Sibson, R. H. (2003), Thickness of the seismic slip zone, *Bull. Seismol. Soc. Am.*, *93*, 1169–1178.

Sleep, N. H. (1995a), Frictional heating and the stability of rate and state dependent frictional sliding, *Geophys. Res. Lett.*, *22*, 2785–2788.

Sleep, N. H. (1995b), Ductile creep, compaction, and rate and state dependent friction within major fault zones, *J. Geophys. Res.*, *100*, 13,065–13,080.

Sleep, N. H. (1997), Application of a unified rate and state friction theory to the mechanics of fault zones with strain localization, *J. Geophys. Res.*, *102*, 2875–2895.

Sleep, N. H. (1999), Rate- and state-dependent friction of intact rock and gouge, *J. Geophys. Res.*, *104*, 17,847–17,855.

Tinti, E., A. Bizzarri, A. Piatanesi, and M. Cocco (2004), Estimates of slip weakening distance for different dynamic rupture models, *Geophys. Res. Lett.*, *31*, L02611, doi:10.1029/2003GL018811.

Tinti, E., P. Spudich, and M. Cocco (2005), Earthquake fracture energy inferred from kinematic rupture models on extended faults, *J. Geophys. Res.*, *110*, B12303, doi:10.1029/2005JB003644.

Wibberley, C. A. J., and T. Shimamoto (2003), Internal structure and permeability of major strike-slip fault zones: The Median Tectonic Line in mid prefecture, southwest Japan, *J. Struct. Geol.*, *25*, 59–78.

————————————
A. Bizzarri, Istituto Nazionale di Geofisica e Vulcanologia, Sezione di Bologna, Via Donato Creti, 12, I-40128 Bologna, Italy. (bizzarri@bo.ingv.it)

M. Cocco, Istituto Nazionale di Geofisica e Vulcanologia, Sezione di Sismologia e Tettonofisica, Via di Vigna Murata, 605, I-00143 Rome, Italy.